HARVARD-SMITHSONIAN CENTER FOR ASTROPHYSICS
60 Garden Street, Cambridge, MA 02138

Date: 30 October 2006

To: Emilio Falco

Cc: Daniel Fabricant, Brian McLeod, Andrew Szentgyorgyi

From: Deborah Woods

RE: FLWO 48" mirror wavefront sensor test results

Abstract

This memo describes the results of Shack-Hartmann wavefront sensor measurements of the 48" mirror at the Whipple Observatory, Mount Hopkins, AZ. The observations show significant errors in the figure of the primary mirror. Visual inspection of the data shows spots that are significantly shifted, distorted in shape, and some spots that are missing entirely from the images. Local slope errors on the mirror surface are as large as 1.6 arcsec, and vary in direction and magnitude from one location to another. The severity of the local slope errors precludes measurement of the large scale aberrations. Our conclusion is that the 48" mirror is significantly flawed.

Introduction

We built a Shack-Hartmann wavefront sensor to characterize the 48" telescope mirror at the Whipple Observatory, Mount Hopkins, AZ. A Shack-Hartmann wavefront sensor functions by projecting a wavefront from the primary mirror onto a lenslet array. The lenslet array divides the incoming wavefront into different subapertures, corresponding to different spatial samples of the primary mirror. The lenslets focus the incoming wavefront into a grid of spots that is imaged on a CCD detector. The lateral positions of the spot images on the detector can be traced to the local tilt of the incoming wavefront at the particular lenslets. Deviations from nominal positions of the spot images correspond to local slope errors in the primary mirror. Figure 1 illustrates the principle of the Shack-Hartmann wavefront sensor.

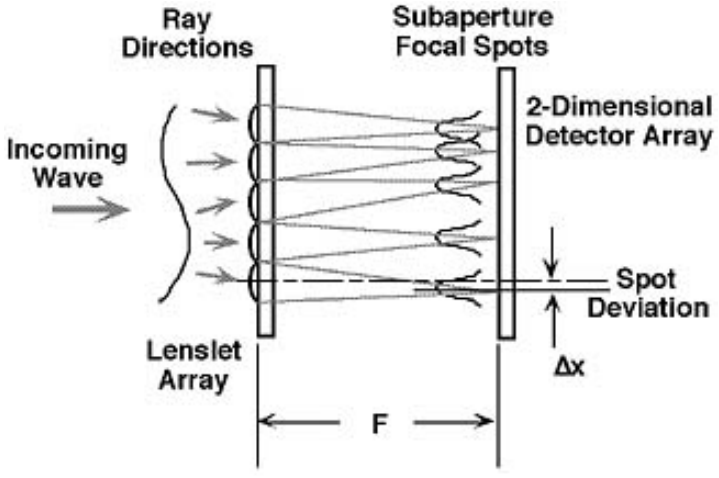

Figure 1: A Shack-Hartmann wavefront sensor transforms the local tilt of the incoming wavefront to lateral shifts in the positions of subaperture focal spots [1].

The wavefront sensor that we built for the 48" telescope consists of a linear slide that moves between aperture for sky or an LED and pinhole for calibration, an achromatic lens to collimate the light, a lenslet array, and a CCD camera for imaging. There is also a fold mirror to send half of the light beam to another achromatic lens that focuses onto a video camera for star acquisition. Figure 2 shows the optical layout of the 48" telescope wavefront sensor, and Figure 3 gives the optical prescription of the system.

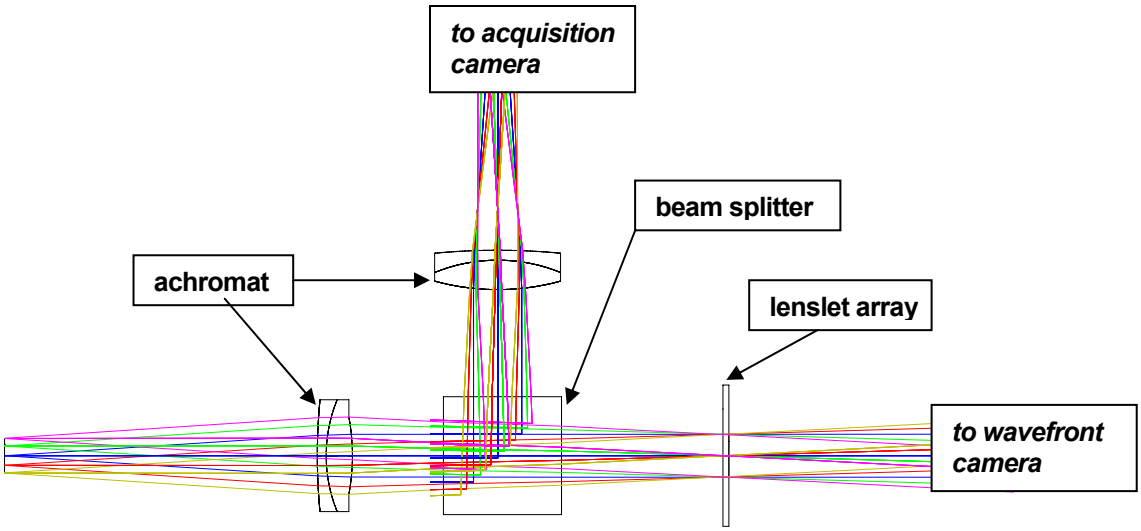

Figure 2: Optical layout of wavefront sensor. Light enters the system from the left.

System/Prescription Data (units of mm)

File : C:\ZEMAX\Deborah\wfs-48inch\48inch-I-0400-53.zmx
Title: 48 INCH TELESCOPE
Date : MON OCT 30 2006

SURFACE DATA SUMMARY:

Surf	Type	Comment	Radius	Thickness	Glass	Diameter	Conic
OBJ	STANDARD		Infinity	Infinity		0	0
STO	STANDARD	PRIMARY MIRROR	-4591.814	-1716.757	MIRROR	1219.225	-1.040231
2	STANDARD	SECONDARY MIRROR	-1532.688	1716.757	MIRROR	310.295	-3.083152
3	STANDARD	TO START OF WFS	Infinity	601.1001		89.58369	0
4	STANDARD	TO FOCAL POINT	Infinity	53.028		12.65453	0
5	STANDARD	FOCAL POINT	Infinity	52.93628		5.877529	0
6	STANDARD	ACHROMAT - LAO068	100.5328	1.499997	SF5	19	0
7	STANDARD	BACK OF ACHROMAT	25.13005	4.439996	SK11	19	0
8	STANDARD		-35.99063	15.4		13.15235	0
9	STANDARD	MIMIC BEAM SPLI	Infinity	20	BK7	20	0
10	STANDARD	DISTANCE TO PUPIL	Infinity	27.326		19	0
11	USERSURF	LENSLET ARRAY	28.4226	1	BK7	23.99995	0
12	STANDARD		Infinity	53		7.305918	0
IMA	STANDARD	FOCAL POINT	Infinity			10.23976	0

Figure 3: Optical prescription of wavefront sensor.

The resolution of the wavefront sensor to small scale aberrations on the primary mirror is determined by the size of subapertures sampled on the mirror. The size of subapertures sampled in turn depends on the diameter of the collimated light beam for the telescope – wavefront sensor system and the pitch of the lenslet array. The lenslet array that we chose has a pitch of 0.400 mm and a focal length of 53 mm (model 400-53-S from Adaptive Optics Assoc.). This lenslet array, along with a 56 mm focal length achromat, produces the smallest scale sampling of any commercially available array while maintaining a nearly 1:1 image scale between the telescope focal plane and the spot images. The 56 mm focal length achromat, located one focal length back from the focal point of the F/7.72 telescope beam, results in a pupil diameter of 7.2 mm. The number of subapertures imaged equals the diameter of the pupil / diameter of a lenslet = 7.2 mm / 0.400 mm = 18 subapertures. The diameter of a region sampled on the primary mirror is thus 1200 mm / 18 = 60 mm. The 60 mm resolution is on the order of the expected scale of the aberrations based on previous measurements by B. McLeod and E. Falco [2, 3].

The slope error on the primary mirror across an individual subaperture relates to the lateral shift of the imaged subaperture spot on the detector according to:

(1) $\tan \theta \approx \theta \approx (½)\, \Delta x / m\, f_{eff}$ [radian]

or, equivalently:

(2) $\theta \approx ½\, \Delta x / m\, p_{mas}$ [arcsec]

where θ is the slope error on the mirror surface, m is the demagnification of the lenslet array – achromat system (53 mm / 56 mm = 0.95), Δx is the measured lateral shift in spot position, f_{eff} is the effective focal length of the telescope system (9.37 m), p_{mas} is the plate scale (45.45 µm/arcsec), and the factor of ½ is because the angular displacement of the reflected wavefront is twice that of the incident wavefront. Note that the detector has 20 µm pixels, i.e. a lateral shift of one pixel corresponds to a slope error on the mirror of 0.24 arcsec.

Observations and Analysis

Our reference grid shows the LED imaged through the pinhole aperture, which is located at the focal point of the telescope. This image provides a reference for the nominal spot positions, imaged by the lenslet array onto the detector. Figure 4 shows that the reference spots are distributed uniformly on the detector.

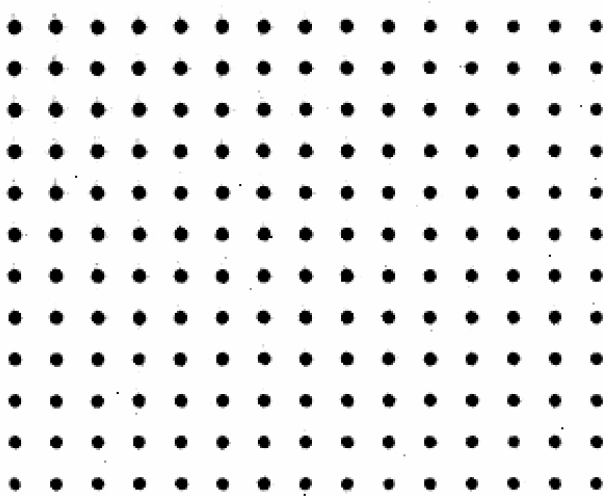

Figure 4: Reference grid of LED light imaged by lenslet array.

Observations with the wavefront sensor at the 48" telescope took place on 16 June 2006. Present at the telescope were Emilio Falco, Andrew Szentgyorgyi, Ted Groner, and Wayne Peters. Deborah Woods and Tim Pickering participated in the observations and analysis remotely. We first acquired calibration data to determine the orientation of the wavefront sensor images with respect to the primary mirror and to the sky. In the images shown below, north is up and east is to the right. Figures 5 and 6 show images of the primary mirror in terms of the subaperture spots measured by the wavefront sensor for different telescope orientations (where (alt, az) = (33.11, -59.03) and (88.05, 155.76), respectively.)

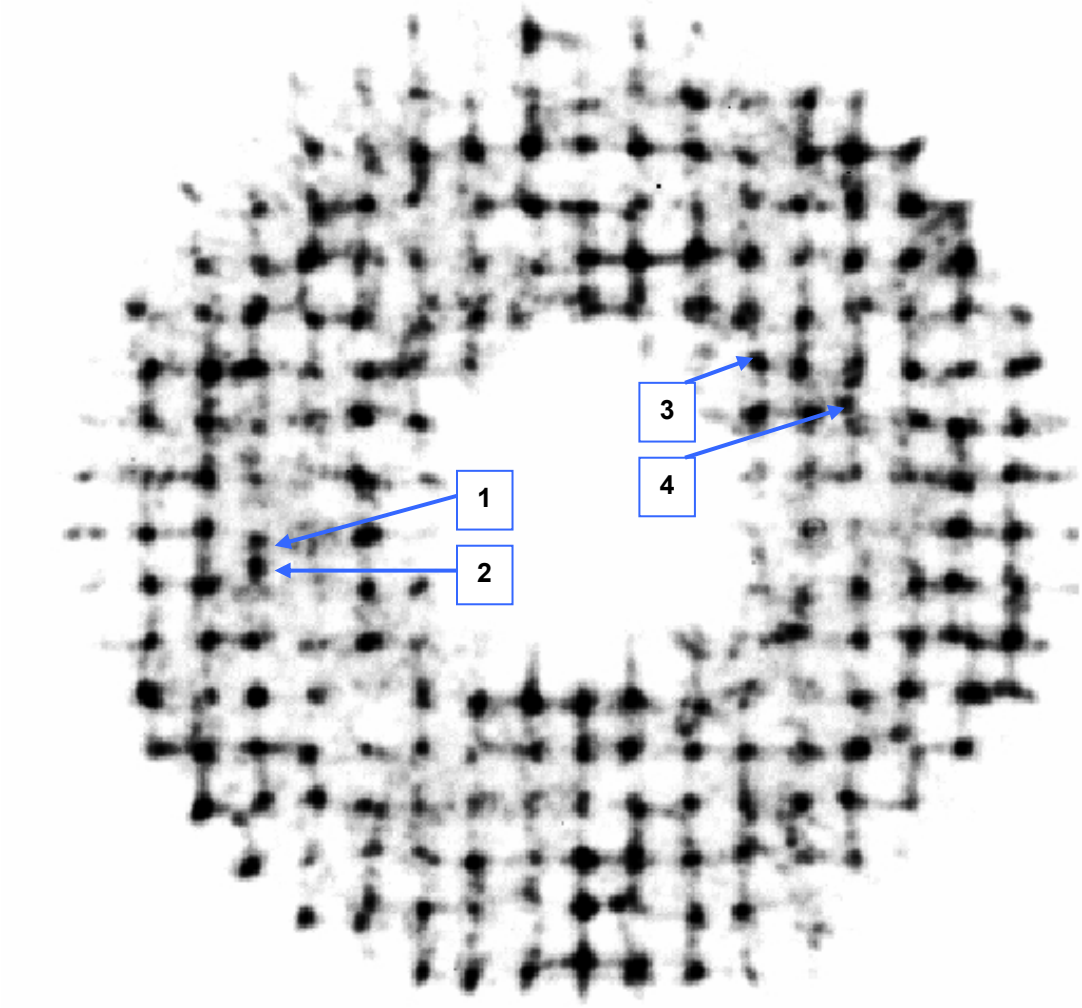

Figure 5: Wavefront sensor image of subaperture spots for the telescope pointing at (alt, az) = (33.11, -59.03). The spots indicated with the blue arrows are visibly shifted from their nominal positions, indicating significant slope errors in the primary mirror.

The measured slope errors on the mirror surface for subaperture spots indicated with the blue arrows in Figure 5 are given in Table 1. These slope errors, measured solely from the lateral shifts from nominal spot positions, can be taken as a lower limit on the mirror deformity because variations in spot shape and intensity are also present. The slope errors on the mirror surface are calculated using Equation (2). The slope errors are over a subaperture region corresponding to 60 mm on the mirror.

We measure the subaperture spots' lateral shift from nominal position using standard *IRAF* astrometry. First, we find the offset between the reference grid and the wavefront sensor observation (x_{offset}, y_{offset}) by measuring the centroids of a representative set of subaperture spots and of the corresponding reference spots. The subaperture spots are chosen visually to have small or undetectable shifts out of line with their neighbors. We use the *IRAF* task "center" to measure the centroid of the subaperture spot (x_{obs}, y_{obs}) and the reference spot (x_{ref}, y_{ref}). The offset is determined from the mean difference between subaperture and reference spot positions. The lateral shift $\Delta x = x_{ref} - x_{obs} - x_{offset}$, and similarly for Δy.

ID	Δx (pixel)	$\pm \Delta x$ (pixel)	Δy (pixel)	$\pm \Delta y$ (pixel)	Δr (pixel)	Δr (μm)	surface error (arcsec)	± surface error (arcsec)
1	0.42	0.058	4.66	0.060	4.67	93.50	**1.08**	0.02
2	0.60	0.051	-6.32	0.061	6.34	126.89	**1.47**	0.02
3	-4.21	0.057	-1.48	0.056	4.46	89.21	**1.03**	0.02
4	3.87	0.070	-5.94	0.072	7.09	141.77	**1.64**	0.02

Table 1: Local slope errors on the mirror surface measured from subaperture splot displacement.

The subaperture spots show significant variations in intensity, in addition to lateral shifts in position. In Figure 6, we show a wavefront sensor image with regions circled in red to call attention to the subaperture spots that are missing entirely from the image. The spots are either so far out of focus that they do not appear at all, or they correspond to locations on the primary mirror with unusual surface damage. Figure 7 shows a picture of the primary mirror with visible damage, for comparison with the wavefront sensor image. We note that the wavefront sensor image and the photo of the mirror are displayed so that a physical region on the mirror corresponds to the same location in the wavefront sensor image, e.g. the top right corner of the photo is mapped to the top right corner of the wavefront sensor image. The actual mapping of a physical region on the mirror to the location of a subaperture spot in the wavefronte sensor image is inverted, e.g. the north-east edge of the mirror is mapped to a spot on the south-west edge of the image plane.

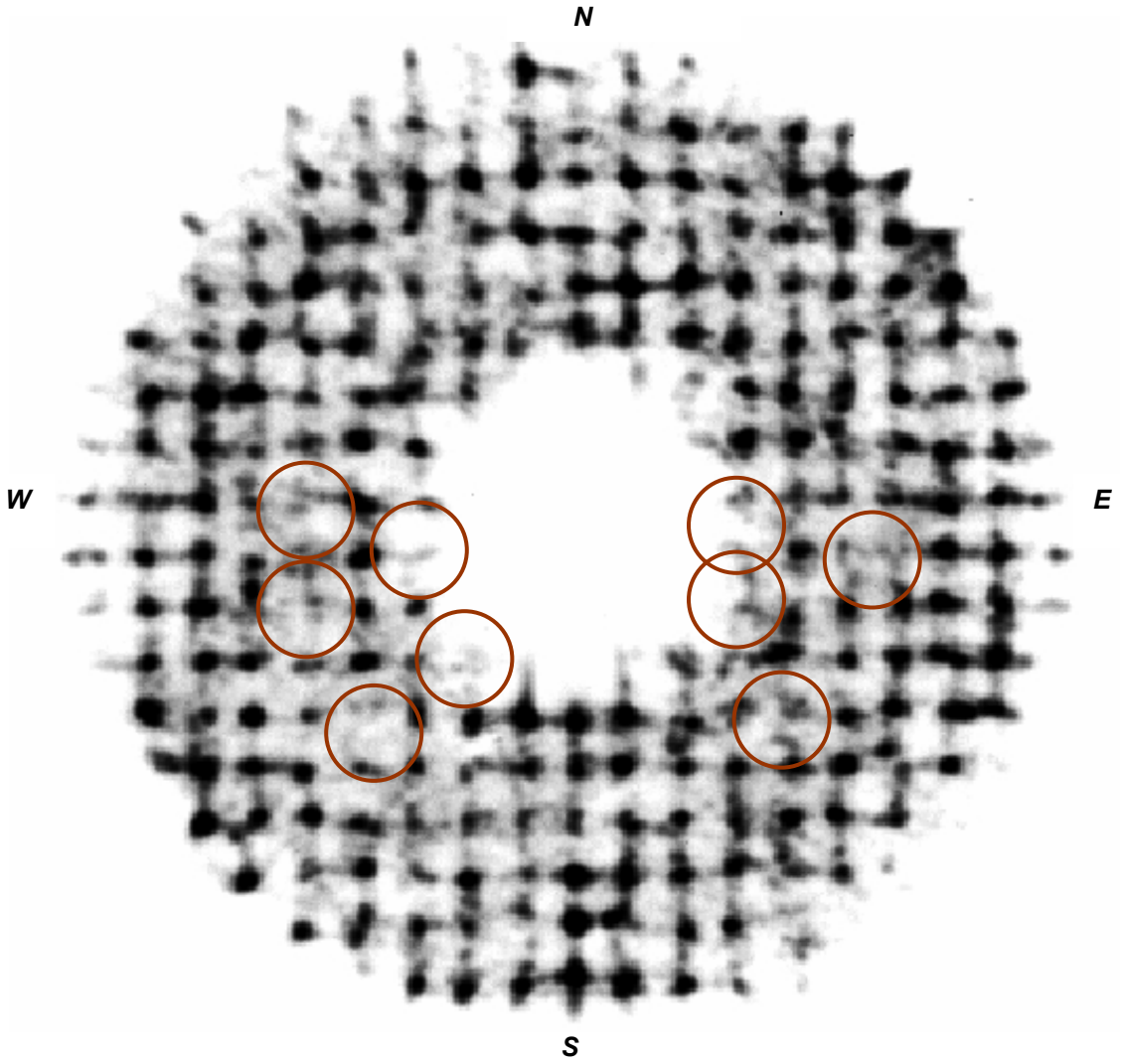

Figure 6: Wavefront sensor image of subaperture spots for the telescope pointing at (alt, az) = (88.05, 155.76). The regions circled in red appear to missing spots, which could either be completely out of focus or otherwise not reflected properly by the mirror. The image is oriented so that north on the sky is up and east is to the right.

In Figure 7, we show a photo of the primary mirror surface. A few of the damaged regions show up easily against the reflection of the dome ceiling. We call attention to the regions circled in red because those physical locations on the mirror match up well with the locations of missing subaperture spots in the wavefront sensor image. It appears that the mirror fails to properly reflect light from the source star in the corresponding subapertures of the wavefront sensor. The damaged regions of the mirror not only fail to properly reflect source light, but also it is possible that the regions may be responsible for scattered light in the telescope system.

S

E

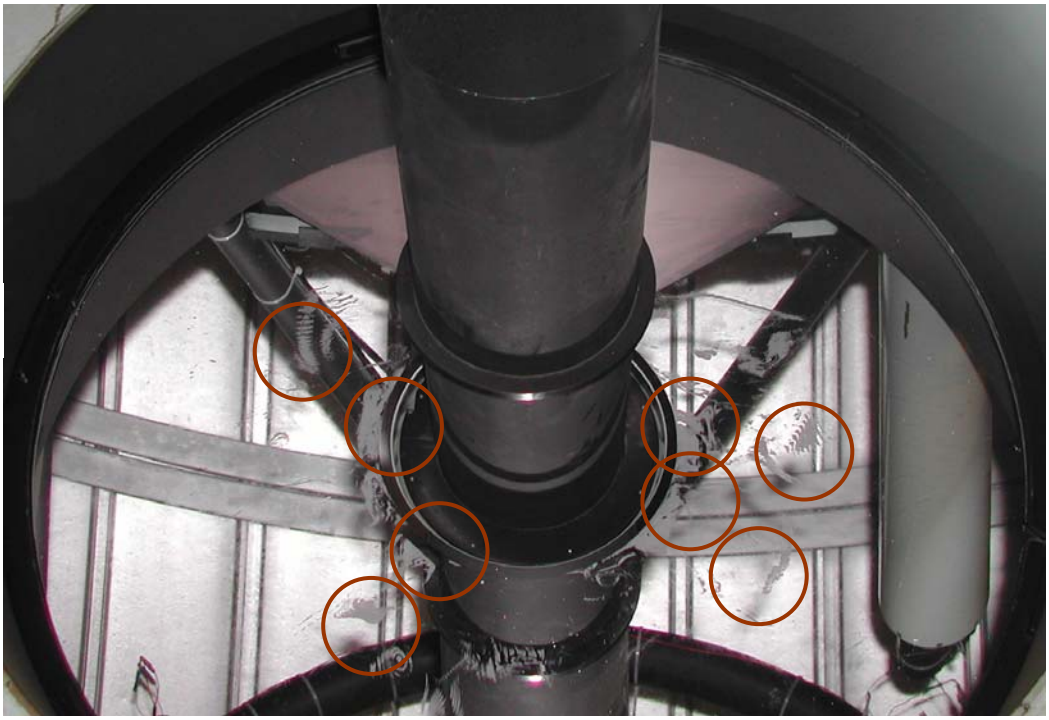

W

N

Figure 7: The mirror is oriented so that north is at the bottom of the image. In the orientation pictured, the region of the mirror in the top right corner of the photo corresponds to a subaperture spot in the top right corner of the wavefront sensor image, for example.

The wavefront sensor images in Figures 5 and 6 demonstrate that the position, intensity, and shape of the subaperture spots vary enormously from one spot to the next. The spots indicated with blue arrows are visibly shifted far from their nominal positions. The regions circled in red are missing spots entirely. Comparison with the reference image (Figure 4) confirms that the mirror is responsible for the shifted and absent subaperture spots. We do not detect a correlation between wavefront errors and telescope orientation, but it is not possible to rule out a correlation given the limitations of the analysis.

Wavefront analysis and reconstruction is not accurate for these images because local slope errors cannot alone describe the observed subaperture spot positions and variations in intensity. The local aberrations are severe enough to interfere with measurement of the low frequency aberration terms. However, we report in Figure 8 an example wavefront analysis in order to demonstrate the scale of the errors. Table 2 lists the derived RMS wavefront errors and Table 3 lists the Zernike coefficients for a representative set of observations. The wavefront analysis is performed using a modified version of the MMT wavefront sensor analysis software written by T. Pickering et al. [4].

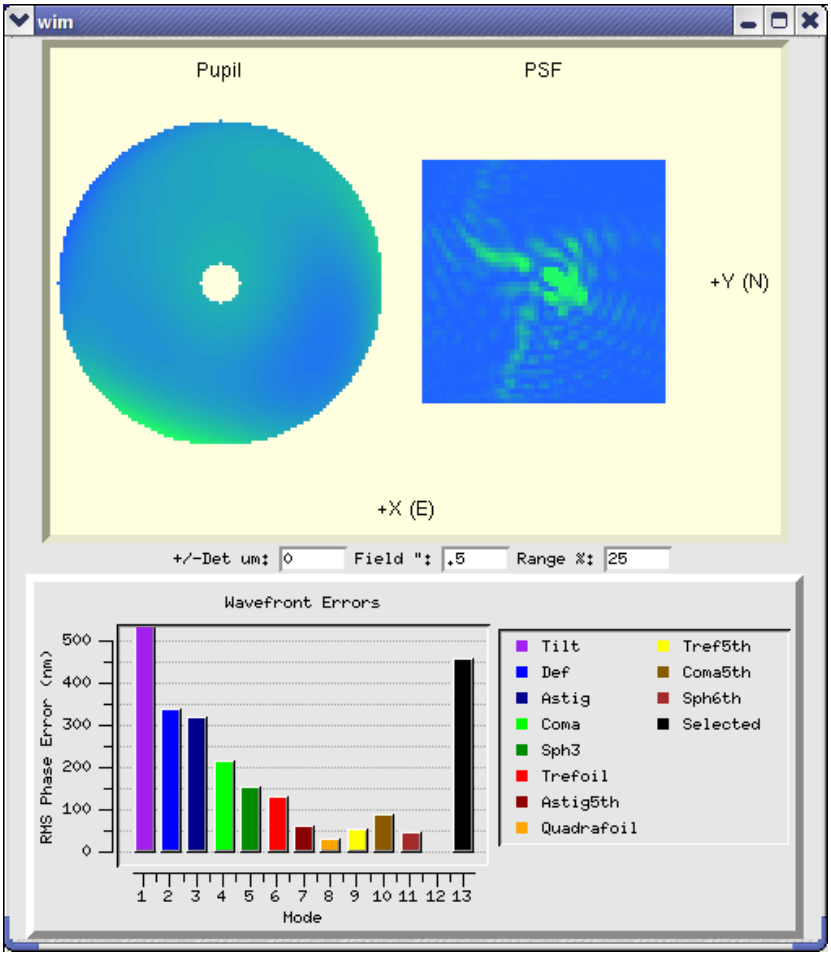

Figure 8: Example wavefront analysis. The figure on the top left represents the wavefront errors of the pupil, and the top right shows the expected PSF. Images and wavefront analysis are produced by a modified version of the MMT wavefront sensor analysis software [4].

RMS Wavefront Errors (nm)	
Tilt	22000
Defocus	270
Astig	300
Coma	250
Spherical 3rd	150
Trefoil	125
Astig 5th	55
Quadrafoil	45
Trefoil 5th	65
Coma 5th	85
Spherical 6th	45

Table 2: Mean RMS Wavefront Errors for a representative set of observations.

Zernike term	Description	Minimum (nm)	Maximum (nm)	Mean value (nm)	Std. Dev. (nm)
z1	tilt y-axis	-39249	-30350	-35073.7	2227.85
z2	tilt x-axis	-27436	-20049	-24833	1703.73
z3	defocus	-5039	853	-203.545	1748.8
z4	astig – 45	-794	764	-203.545	427.047
z5	astig – 0	-990	3926	837.455	1808.67
z6	X-coma	266	2978	1104.95	716.126
z7	Y-coma	-489	2609	211.273	571.769
z8	spherical	-610	797	327.682	275.379
z9	trefoil-bsX	-1808	306	-433.909	597.661
z10	trefoil-bsY	117	2354	519.182	502.75
z11	astig 5th – 45	-209	721	84.9091	267.823
z12	astig 5th – 0	-3216	1233	-147.182	924.966
z13	frth – 1	-409	208	-43.0909	162.389
z14	frth – 2	-1713	210	-226.864	162.389
z15	trefoil 5th – X	-91	1854	-226.864	607.477
z16	trefoil 5th – Y	-1002	596	77.4091	297.648
z17	X-coma 5th	-1087	311	-215.636	297.648
z18	Y-coma 5th	-2023	736	4.09091	531.954
z19	spherical 6th	-665	561	-4.31818	308.813

Table 3: Zernike coefficients for the full set of observations.

Conclusion

Observations with a Shack-Hartmann wavefront sensor of the 48" telescope mirror at Mount Hopkins, AZ, show that the mirror has severe deformations in its surface. Deviations on the scale of ~60 mm produce subaperture spot images that are significantly shifted in position, vary in intensity, and are in some cases are entirely absent. Local slope errors on the mirror are on the order of 1.5 arcsec. Large scale aberrations may also be present, but the magnitude of the small scale aberrations precludes their measurement.

References

[1] Platt, B. C. & Shack, R. "History and Principles of Shack-Hartmann Wavefront Sensing", Journal of Refractive Surgery, Sept./Oct. 2001, Vol. 17.

[2] McLeod, B. A. "Status of 1.2m Optical Quality" 21 May 1999.

[3] Falco, E. E. McLeod. B. A. "Low order aberrations of the FLWO 1.2 m" 6 June 2000.

[4] Pickering, T. E., West, S. E. & Fabricant, D. G. "Active optics and wavefront sensing at the upgraded 6.5-meter MMT" SPIE, 2004, Vol. 5489, 1041.